

# Magnesium Powder Injection Molding (MIM) of Orthopedic Implants for Biomedical Applications

M. WOLFF,<sup>1,5</sup> J.G. SCHAPER,<sup>2</sup> M.R. SUCKERT,<sup>3</sup> M. DAHMS,<sup>3</sup>  
T. EBEL,<sup>1</sup> R. WILLUMEIT-RÖMER,<sup>1</sup> and T. KLASSEN<sup>4</sup>

1.—Helmholtz-Zentrum Geesthacht, Centre for Materials and Coastal Research, Institute of Materials Research, Div. Metallic Biomaterials, Max-Planck Str.1, 21502 Geesthacht, Germany. 2.—Element22 GmbH, Wischhofstr. 1-3, Geb. 13, 24148 Kiel, Germany. 3.—University of Applied Sciences, FH-Flensburg, Kanzleistr. 91-93, 24943 Flensburg, Germany. 4.—Helmut Schmidt University, Holstenhofweg 85, 22043 Hamburg, Germany. 5.—e-mail: martin.wolff@hzg.de

Metal injection molding (MIM) has a high potential for the economic near-net-shape mass production of small-sized and complex-shaped parts. The motivation for launching Mg into the MIM processing chain for manufacturing biodegradable medical implants is related to its compatibility with human bone and its degradation in a non-toxic matter. It has been recognized that the load-bearing capacity of MIM Mg parts is superior to that of biodegradable polymeric components. However, the choice of appropriate polymeric binder components and alloying elements enabling defect-free injection molding and sintering is a major challenge for the use of MIM Mg parts. This study considered the full processing chain for MIM of Mg–Ca alloys to achieve ultimate tensile strength of up to 141 MPa with tensile yield strength of 73 MPa, elongation at fracture  $A_f$  of 7% and a Young's modulus of 38 GPa. To achieve these mechanical properties, a thermal debinding study was performed to determine optimal furnace and atmosphere conditions, sintering temperature, heating rates, sintering time and pressure.

## INTRODUCTION

Mg has become very attractive as a lightweight construction material in automotive and consumer applications due to its fuel-saving potential.<sup>1–3</sup> In addition, current research indicates that Mg is suitable for future biomedical orthopedic and traumatology applications.<sup>4–11</sup> Mg is biodegradable and biocompatible and shows mechanical properties matching those of cortical bone tissue.<sup>12,13</sup> Hence, Mg implants do not show stress-shielding problems in contrast to current permanent implant materials such as titanium, stainless steel or cobalt chromium. Stress shielding causes bone resorption and implant loosening.

Mg-based implants are more appropriate for load-bearing applications than degradable polymers, as polymer implants such as polyglycolic acid (PGA) or polylactide acid (PLA), which have inferior mechanical properties<sup>14</sup> and during degradation release acidic degradation products to the human body. In comparison, Mg degrades under alkaline conditions

which stimulates osteoconductivity.<sup>15</sup> Mg-based implants show significant potential to substitute for polymer-based implants produced by a similar injection molding technique as shown in Fig. 1.

The powder metallurgical (PM) processing of Mg is advantageous as this gives rise to homogeneous distribution of elements and a fine-grained microstructure. Metal injection molding (MIM) enables the generation of small and complex-shaped implants on an industrial scale with a high level of automation and reproducibility. Moreover, this economic near-net-shape production route enables the generation of both nearly dense as well as porous structures which promote vascularization and cell ingrowth into the degrading implant (osteointegration).<sup>10</sup> However, the advantages and disadvantages of porous Mg alloy parts for biomedical applications are currently controversial and their merits are still under debate.<sup>16,17</sup> A major challenge for Mg PM is the strong affinity of Mg to oxygen that leads to the formation of a stable oxide layer on the powder particle surface which acts as a diffusion barrier

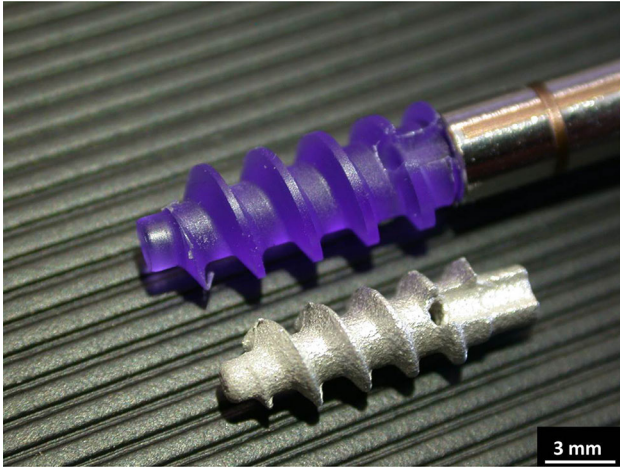


Fig. 1. Suture anchor screws made by injection molding technique using the same mold: upper screw made from poly L-lactide/DL-lactide copolymer (PLDLA), courtesy: Conmed Linvatec; lower screw made from Mg-0.9Ca powder blend by MIM at Helmholtz-Zentrum Geesthacht.

and inhibits sintering. In order to overcome this challenge, several approaches have been considered in recent years.<sup>18–22</sup>

This study focuses on the improvement of the full process chain of MIM of Mg alloys. The selection of an adequate polymer binder system that does not react with magnesium during thermal debinding and sintering is mandatory for successful processing.

Hence, the influence of different backbone polymers on sintering and on the mold-filling ability during injection molding will be discussed. Moreover, the effect of different furnace atmospheres and pressure during thermal debinding and sintering will be integrated within this study. In doing so, biodegradable Mg-0.9Ca implants with sufficient mechanical strength up to 141 MPa ultimate tensile strength (UTS), 73 MPa tensile yield strength (TYS) and 38 GPa Young's modulus can be produced successfully using MIM.

## MATERIALS AND METHODS

### Powder and Feedstock Preparation

The base material, a Mg-0.9Ca powder mixture, was prepared by blending pure spherical Mg powder (SFM; Martigny, Switzerland) with a gas-atomized Mg-10Ca master alloy powder (MAP) (ZfW; Clausthal, Germany) in a planetary mixer by stirring the components for 5 min (Thinky ARE-250 planetary mixer; Japan). To avoid any oxygen uptake, the complete powder and specimen were handled under a protective argon atmosphere in a glovebox (Unilab; MBraun, Germany). The powder blend was used for the feedstock preparation as well as for the preparation of a binder-free reference specimen. To enable the shaping of the part via

MIM, different organic polymer binders as shown in Table I were mixed with the Mg–Ca powder. The Thinky mixer was also used for the feedstock preparation.

### Metal Injection Molding (MIM), Debinding and Sintering

MIM of Mg-0.9Ca feedstock was processed using an industrial injection molding machine (Arburg Allrounder 320S) to produce a dog bone-shaped MIM tensile test specimen according to ISO 2740 and rectangular bars for the measurement of the dynamic Young's modulus. The different bone screw demonstrators, as shown in Figs. 1 and 2, were also prepared. The solvent debinding of the organic wax components and stearic acid was performed in hexane at 45°C for 10–15 h (Lömi EBA50/2006, Germany). Thermal debinding and sintering was conducted in a combined debinding and sintering hot wall furnace (Xerion XRetort; Germany).

The thermal debinding was conducted in a reactive Ar + 5% H<sub>2</sub> gas flow of 0.5 L/min at 5–20 mbar which include 6 cycles of alternating pressure between 5 and 800 mbar as shown in Fig. 3.

The sintering time of the parts was 64 h at ambient pressure in a protective high purity argon 6.0 (Ar 6.0) atmosphere. Mg has the highest vapor pressure of all technical metals and thus it cannot be sintered under high vacuum conditions. Since debinding and sintering under vacuum conditions is paramount to achieve a residual-free thermal debinding, some sintering experiments were performed under vacuum condition up to a maximum sintering time of 2–4 h at 630–645°C.

### Materials Characterization

The shrinkage and the residual porosity of the sintered parts were investigated using the Archimedes method (Sartorius LA230S; Germany), geometrical data calculation (Mahr 16EX calliper; Germany) and scanning electron microscopy (SEM) equipped with energy dispersive x-ray (EDX) (Zeiss DSM 962; Germany). The microstructure was investigated using optical light microscopy (Olympus PGM 3) and SEM. The rectangular bars were used for the non-destructive measurement of the dynamic Young's modulus using resonant ultrasonic spectroscopy (RFDA; IMCE, Belgium). The tensile tests of the sintered MIM Mg-0.9Ca specimen were conducted on a Schenck Trebel RM100 materials testing machine.

## RESULTS AND DISCUSSION

### Sintering Time

The dependence of the densification of binder-free Mg sinter parts on sintering time is shown in Fig. 4. The residual porosity of the green part, pressed at 100 MPa, is approximately 20%. The diagram

**Table I. List of wax, additive and polymer components used for the feedstock preparation**

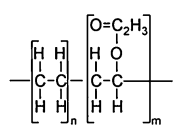
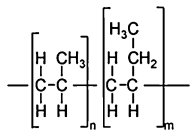
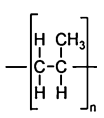
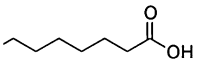
<u>Binder—no.</u>	<u>Binder</u>	<u>Full name</u>		<u>Manufacturer</u>
1	PE-VA	Polyethylene-vinylacetate		Bassell
2	PPco1PB	Polypropylene-copolymer polybutylene		Sigma-Aldrich
3	PP	Polypropylene		
4	PW55	Paraffin wax		Merck
5	PW65	Paraffin wax		Fisher scientific
6	StA	Stearic acid		Merck



Fig. 2. Bone screw demonstrator made with Mg-0.9Ca feedstock using MIM. Parts (bottom to top) green part after MIM, solvent debond green part and sintered part.

shows that a minimum sintering time around 8 h is required for the initial necking phase to occur during sintering.

This is a relatively long time when compared with other oxygen affine sintering materials, e.g., titanium. The reduction of porosity during sintering occurs slowly. The sluggish sintering process is due

to a high affinity of Mg to oxygen, and the oxide layer formed on the powder particle surface acts as a diffusion barrier. Hence, consolidation of the part at ambient pressure is time consuming due to the solid Mg oxide layer having to be partially destabilized and reduced by Ca-rich liquid phases and then moved through the sintering neck growth. This process can be accelerated using vacuum instead of ambient pressure as illustrated below.

### Sintering Pressure and -Atmosphere

Information about furnace atmosphere and furnace pressure is given in Figs. 3 and 5. Sintering of binder-free parts in the furnace runs 1a and 2a in Fig. 5 were carried out in Ar 6.0 atmosphere. In comparison, runs 1b and 2b were carried out in Ar 4.6 which has a lower purity than Ar 6.0. However, a significant difference in the sintering ability of the Mg parts as a function of the furnace gas during sintering cannot be observed in this experiment. On the other hand, significant differences can be observed when runs 1a and 1b are compared with runs 2a and 2b.

Runs 1a and 1b were conducted in vacuum during the heat-up phase. Ar with ambient atmosphere pressure (1013 mbar) was not injected until the sintering temperature was achieved. In comparison,

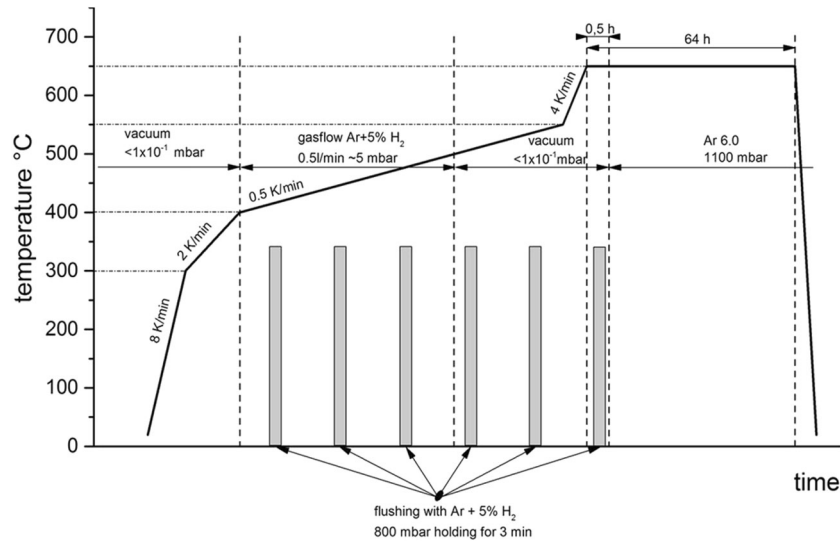


Fig. 3. Time–temperature–pressure diagram of the magnesium sintering process for MIM parts.

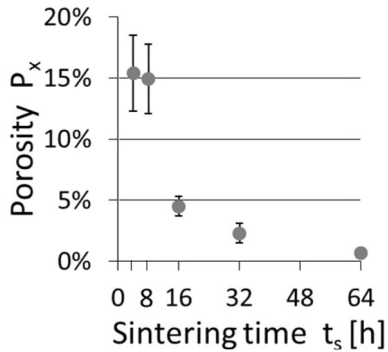


Fig. 4. Residual porosity  $P_x$  of sintered and binder free Mg-0.9Ca cylinders with sintering time  $t_s$ . Sintering temperature  $T_s$  was 630°C at ambient pressure in Ar 6.0 atmosphere.

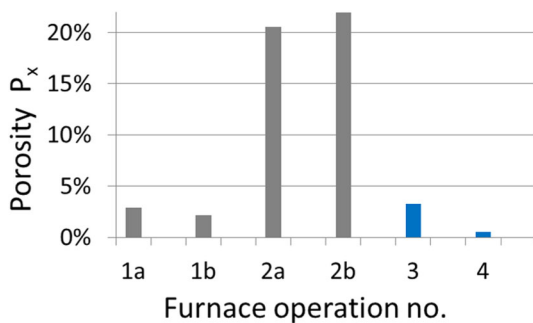


Fig. 5. Residual porosity  $P_x$  of sintered and binder-free Mg-0.9Ca cylinders with change in sintering conditions (furnace pressure, gas quality, sintering time  $t_s$ ). Sintering temperature  $T_s$  was 635°C.

runs 2a and 2b were completely conducted under ambient pressure of Ar gas. Figure 5 shows that heating under a vacuum resulted in lower porosities. In addition, furnace run 3 illustrates the effect of a short sintering time of 2 h under vacuum. The combined effect of vacuum sintering for a short time

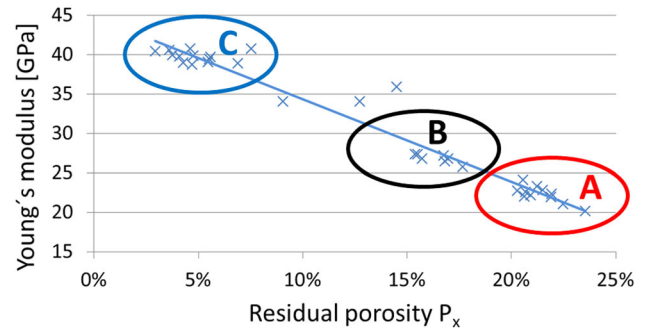


Fig. 6. Linear relationship between residual porosity and Young's modulus of sintered MIM Mg-0.9Ca parts and its dependence on furnace atmosphere and sintering time  $t_s$ . (a) 2 h vacuum sintering at 635°C; (b) 4 h vacuum sintering at 635°C; (c) 2 h vacuum sintering at 645°C + 62 h sintering at ambient pressure in argon.

(2 h), with an additional longer time (62 h) sintering in ambient atmospheric conditions in run 4, produced nearly dense parts with 0.7% residual porosity.

### Sintering of MIM Parts

Application of the vacuum sintering as described in the previous section also improved the dynamic Young's modulus of the binder containing MIM Mg specimen (Fig. 6).

Figure 6 shows the linear dependency between the residual porosity of the sintered MIM part and its Young's modulus.<sup>22</sup> The extrapolation of the linear graph onto the axis of ordinates illustrates that the material would show an elastic modulus of around 45 MPa in fully dense condition. This equivalent to the Young's modulus has been reported for conventionally cast Mg alloys. MIM specimens in regions A and B were sintered for 2 h and 4 h under a vacuum. Specimens in region C underwent an additional 62 h of sintering under ambient



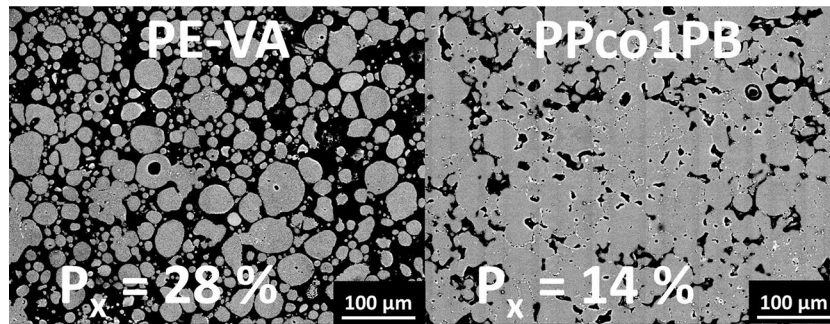


Fig. 7. SEM image of the microstructures of sintered Mg-0.9Ca material. Left image PE-VA was used in comparison to (right image) PPco1PB.

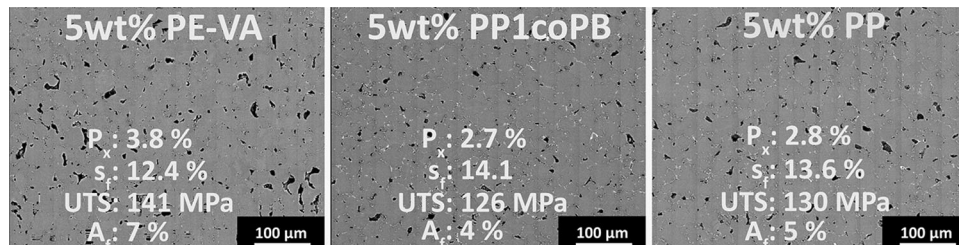


Fig. 8. SEM micrographs of thermal debonded and sintered MIM specimen, showing residual porosity  $P_x$ , shrinkage  $s_f$ , UTS and elongation at fracture  $A_f$  as a function of the used backbone polymer.

atmospheric conditions following the 2 h of sintering under a vacuum. The use of a vacuum at sintering temperatures leads to the evaporation of magnesium due to its high vapor pressure. This leads to the deposition of Mg into the cold area of the furnace heat shielding and covers the whole furnace. Therefore, the vacuum segment for the standard sintering run of MIM Mg parts was set to 0.5 h as shown in Fig. 3.

### Evaluation of Binder Polymer

The standard backbone polymer component for MIM of highly reactive metals like, e.g., titanium used at the HZG (Helmholtz-Zentrum Geesthacht [www.hzg.de](http://www.hzg.de)) is a PE-VA copolymer (see Table I). The use of this copolymer results in very good rheological behavior during the injection molding. Hence, a fundamental premise for defect-free green part production without any jetting, blistering or cavity formation is satisfied. However, the main difference between this standard polymer (PE-VA) and the chosen polymer (PPco1PB or PP) is the acetate group in the PE-VA molecular chain (see Table I). Both images in Fig. 7 show the microstructure of sintered Mg-0.9Ca parts after 8 h of sintering time. The microstructure on the left was prepared with the PE-VA backbone polymer. In contrast, as shown in the microstructure on the right in Fig. 7, PPco1PB results in a much lower residual porosity of the compact. It is proposed that Mg may react with the PE-VA copolymer during thermal debinding before the thermal decomposition of the copolymer.

The PPco1PB copolymer with an oxygen-free molecular chain does not influence the ability of sintering Mg in comparison to the oxygen-containing PE-VA. The standard amount of the backbone polymer in the binder system of the feedstock at the HZG is 35 wt.%. Using feedstock with this amount of polymer, the MIM process step became difficult with PPco1PB or PP compared with PE-VA. The use of PPco1PB or PP results in the segregation of the binder components (wax and polymer) due to the lower solubility of paraffin wax in the polymer. The cavities form in the green compact, and technical problems during dosing of the feedstock in the injection molding machine may occur. However, a reduced amount of polymer binder in the feedstock can be used depending on the geometry of the green compact. The minimum amount of polymer is limited by the strength of the brown part after solvent debinding, as a minimum strength is necessary to handle the part then.

Tensile test specimens, rectangular bars for Young's modulus measurement and different bone screw prototypes, could be successfully produced using only 5 wt.% backbone polymer in the binder system instead of 35 wt.%. The microstructures and mechanical properties resultant are shown in Fig. 8.

The use of 5 wt.% of PPco1PB (see Fig. 8, center) results in the lowest residual porosity,  $P_x$ , of the compound and the highest shrinkage,  $s_f$ , of 14.1%. The use of PP as shown in the microstructure on the right in Fig. 8 produces comparable results. However, these specimens did not show the highest UTS and elongation at fracture. The highest UTS and

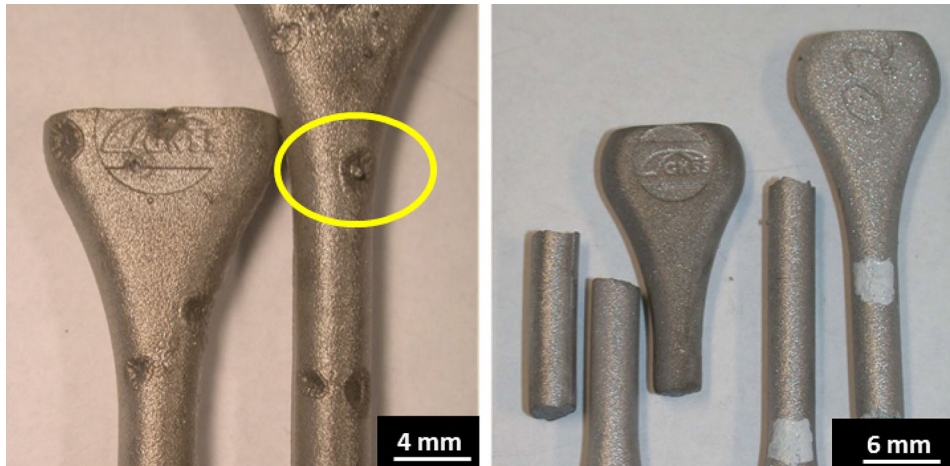


Fig. 9. Left the PPco1PB or PP binders which result in macroscopic defects on the specimen surface. Right these defects cannot be observed when PE-VA binder is used.

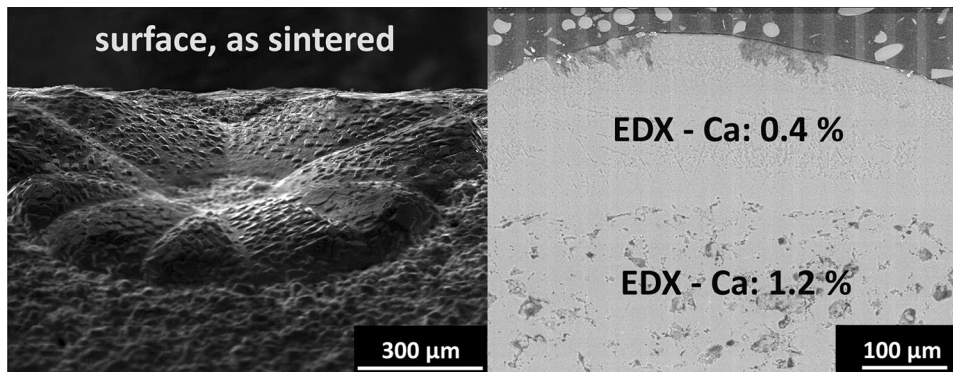


Fig. 10. Left SEM image of the surface of PPco1PB containing tensile test specimen with surface defect. Right cross-section of coarse-grained surface defect showing the Ca concentration measured with EDX.

elongation at fracture  $A_f$  was achieved with PE-VA which has, in comparison to PPco1PB and PP, a higher residual porosity of 3.8% and a lower shrinkage of 12.4%. The inspections of the surface of the tensile test specimens show the reasons behind this discrepancy in Fig. 9. The use of PPco1PB or PP does not harm the ability to sinter Mg which results in a very dense microstructure with low residual porosity. However, these binders cause macroscopic defects on the specimen surface. These defects are probably responsible for the reduced mechanical properties of these parts.

The formation mechanism of these coarse defects on the specimen surfaces is currently unknown. The metallic constituents of all specimens are identical, so differences in the thermal debinding performance of the different polymer binders cause the formation of a liquid phase. Generally, liquid calcium-rich phases occur very locally at temperatures above 515°C. Under normal sintering conditions, these liquid phases wet the whole compact via capillary

forces at the sintering temperature. Figure 10 shows the structure and composition of such surface defects.

The microstructure on the left side of Fig. 10 shows that the defect is mainly a surface effect. However, EDX analysis as shown in the right-hand side of Fig. 10 indicated a Ca content of only 0.4 wt.% inside the structure of the defect in comparison to 1.2 wt.% in the general microstructure of the specimen. The Ca content does not support the assumption of Ca-rich liquid phase segregation to the surface during thermal debinding. To clarify the reasons behind the formation of these defects, short sintering experiments with interrupted thermal debinding will be performed.

## CONCLUSION AND OUTLOOK

Tensile test specimens, Young's modulus test specimens and more complex biomedical implant prototypes have been successfully produced.

Satisfactory mechanical properties have been observed, especially in comparison to polymer-based biodegradable implants. The general feasibility of MIM of Mg alloys has been demonstrated. The main challenge is the protection of the sintered parts from oxygen during the heat treatment. Secondly, an appropriate polymer binder which enables a smooth injection molding operation without any reactions with the metallic components is essential for MIM of Mg. A significant enhancement of mechanical properties was realized using 5 wt.% of backbone polymer in the binder system of the feedstock instead of 35 wt.%. Using this method, mechanical properties such as Young's modulus, tensile strength and elongation matching those of bone tissue and exceeding those of polymer-based biodegradable materials may be achieved. In order to further optimize the mechanical properties, more appropriate backbone polymer binders are needed enabling both failure-free green part production through injection molding techniques while retaining the ability to sinter fine-grained fully dense homogeneous microstructures.

#### REFERENCES

1. H.E. Friedrich and B.L. Mordike, *Magnesium Technology* (Berlin: Springer, 2006).
2. K.U. Kainer, eds., *Magnesium* (Weinheim: Wiley-VCH, 2010).
3. H. Dieringa, N. Hort, and K.U. Kainer, eds., *Proceedings of the Fifth International Light Metals Technology Conference 2011* (Trans Tech Publications Ltd, Material Science Forum, 2011), p 690.
4. Z. Li, X. Gu, S. Lou, and Y. Zheng, *Biomaterials* 29, 1329 (2008).
5. M.P. Staiger, A.M. Pietak, J. Huadmai, and G. Dias, *Biomaterials* 27, 1728 (2006).
6. F. Witte, V. Kaese, H. Haferkamp, E. Switzer, A. Meyer-Lindenberg, C.J. Wirth, and H. Windhagen, *Biomaterials* 26, 3557 (2005).
7. F. Witte, J. Reifenrath, P.P. Müller, H.-A. Crostack, J. Nellesen, F.W. Bach, D. Bormann, and M. Rudert, *Materi-  
alwiss. Werkstofftech.* 37, 504 (2006).
8. F. Witte, F. Feyerabend, P. Maier, J. Fischer, M. Störmer, C. Blawert, W. Dietzel, and N. Hort, *Biomaterials* 28, 2163 (2007).
9. F. Witte, H. Ulrich, M. Rudert, and E. Willbold, *J. Biomed. Mater. Res.* 81A, 748 (2007).
10. F. Witte, J. Fischer, J. Nellesen, H.A. Crostack, V. Kraese, A. Pisch, F. Beckmann, and H. Windhagen, *Biomaterials* 27, 1013 (2006).
11. F. Witte, H. Ulrich, C. Palm, and E. Willbold, *J. Biomed. Mater. Res.* 81A, 757 (2007).
12. G. Poumarat and P. Squire, *Biomaterials* 14, 337 (1993).
13. A.R. Cunha, B Umbelino, M.L. Correia, and M.F. Neves, *Int. J. Hypertens.*, Hindawi Publishing Co. (2012) Art-ID 754250.
14. B. Ratner, A. Hoffmann, F. Schoen, and J. Lemons, eds., *Biomaterials Science: An Introduction to Materials in Medicine* (San Diego: Elsevier Academic Press, 2004).
15. C. Janning, E. Willbold, C. Vogt, J. Nellesen, A. Meyer-Lindenberg, H. Windbergen, F. Thorey, and F. Witte, *Acta Biomater.* 6, 1861 (2010).
16. J. Capek and D. Vojtech, *Mater. Sci. Eng.* 33C, 564 (2013).
17. K. Bobe, E. Willbild, I. Morgenthal, O. Andersen, T. Studnitzky, W. Tillmann, C. Vogt, K. Vano, and F. Witte, *Acta Biomater.* 9, 8611 (2013).
18. M. Wolff, M. Dahms, and T. Ebel, *Adv. Eng. Mater.* 12, 829 (2010).
19. M. Wolff, T. Guelck, and T. Ebel, *Euro PM 2009: Proceeding*, 2, 417 (2009).
20. M. Wolff and N. Hort, *Powder Inject. Mould. Int.* 2, 63 (2008).
21. M. Wolff, C. Bischof, M. Dahms, T. Ebel, and T. Klassen, *9th International Conference on Magnesium and their Applications* (Vancouver, Canada, July 8–12, 2012) p 102.
22. M. Wolff, J.G. Schaper, M. Dahms, T. Ebel, K.U. Kainer, and T. Klassen, *Powder Metall.* 57, 331 (2014).